Toxicology 518 (2025) 154248

Contents lists available at ScienceDirect

Toxicology

journal homepage: www.elsevier.com/locate/toxicol

A high-throughput microphysiological system to quantify key events leading to liver fibrosis

Saskia Schmidt [a,b], Laura Suter-Dick [a,c,*]

[a] School of Life Sciences, University of Applied Sciences and Arts Northwestern Switzerland, Muttenz CH-4132, Switzerland
[b] Department of Pharmaceutical Sciences, University of Basel, Basel CH-4001, Switzerland
[c] Swiss Centre for Applied Human Toxicology (SCAHT), Basel CH-4001, Switzerland

ARTICLE INFO

Keywords:
Liver fibrosis
MPS
AOP
NAMs

ABSTRACT

New approach methodologies (NAMs), including microphysiological systems (MPS), are emerging as alternatives to animal testing. In the liver, chronic hepatocellular damage can progress to fibrosis, which has been described by an Adverse Outcome Pathway (AOP). However, standardized in vitro models that capture and quantify key AOP events and cell-cell interactions are lacking. We developed a scalable liver fibrosis model using the 384-well Akura™ Twin microplate featuring 168 interconnected well pairs. We studied fibrosis progression by seeding HepaRG microtissues (MTs), with or without THP-1 cells in alpha wells and hepatic stellate cell (hTERT-HSC) MTs in beta wells. Cell health and metabolic activity were monitored via specific sensors that detect glucose and lactate levels. Transforming growth factor beta 1 (TGF-β1), methotrexate (MTX) and acetaminophen (APAP) reduced albumin production, indicating hepatocellular injury. TGF-β1 activated THP-1, increasing ALOX5AP, TREM2, and TGF-β1 mRNA expression. PAI-1 protein levels increased following treatment with TGF-β1, particularly in HepaRG-THP-1 co-cultures. In hTERT-HSCs, TGF-β1 also induced expression of fibrosis markers (ACTA2, COL1A1, COL3A1 and FN1) and increased stress fibers and fibronectin expression. Extracellular matrix remodeling was confirmed by elevated Pro-Collagen 1A1 and CTGF protein levels upon TGF-β1 treatment. The Akura™ Twin platform enables high-throughput modeling of liver fibrosis, mimicking the key events of the liver fibrosis AOP. This model, combining a high-throughput MPS with established cell lines, offers a promising tool to investigate fibrosis mechanisms and advancing quantitative AOP development. Journal: Toxicology (Special Issue: Hepatotoxicity: mechanisms and animal-free prediction models).

1. Introduction

New approach methodologies (NAMs) are increasingly being recognized by regulatory authorities such as the European Medicines Agency (EMA) and the U.S. Food and Drug Administration (FDA) as alternatives to traditional animal testing (Edwards et al., 2025; Ingber, 2022). These NAMs include in vitro models such as microphysiological systems (MPS) and organ-on-chip (OOC) platforms, as well as in silico models (Roberts, 2024; Vinken, 2024). The FDA Modernization Act of 2021 has paved the way for the incorporation of NAMs in drug development, driven by ethical concerns and species-species differences affecting safety and efficacy assessments. MPS, including OOCs, incorporate biomimetic strategies like microfluidics (e.g. shear stress, continuous nutrient supply), extracellular matrices that mimic tissue structures (e.g. stiffness, tissue-tissue interactions) and mechanical cues (e.g. mechanical loading to improve bone tissue mineralization) to enhance physiological relevance (Ingber, 2022; Scheinpflug et al., 2023). Mechanistic information for the development of NAMs is often derived from Adverse Outcome Pathways (AOPs), which describe the molecular and cellular mechanisms leading to adverse effects in response to a chemical or pharmaceutical stressor (Vinken, 2024). AOPs are initiated by a molecular initiation event (MIE) that triggers a cascade of key events (KEs), ultimately resulting in an adverse outcome at the organ level (Horvat et al., 2017). Developed as toxicological knowledge frameworks, AOPs aim to aid in the risk assessments of chemicals and pharmaceuticals. The organization for Economic Cooperation and Development (OECD) has established test guidelines based on AOPs that promote in vitro and in silico methods, such as OECD Guideline No. 497, which outlines defined approaches for skin sensitization testing (Casati et al., 2022). However, standardized guidelines and in vitro models for

* Correspondence to: Hofackerstrasse 30, Muttenz CH-4132, Switzerland.
E-mail address: laura.suterdick@fhnw.ch (L. Suter-Dick).

https://doi.org/10.1016/j.tox.2025.154248
Received 15 May 2025; Received in revised form 18 July 2025; Accepted 31 July 2025
Available online 5 August 2025

assessing systemic toxicity, particularly in the liver, remain limited (Vinken, 2024).

Liver toxicity is a major concern in drug development. Since 1969, at least 20 drugs have been withdrawn from the market due to hepatotoxicity, making it the most frequent cause for safety-related drug retractions (Babai et al., 2021; Kullak-Ublick et al., 2017). Among the various forms of liver damage, liver fibrosis represents a critical, progressive condition, characterized by excessive scarring and loss of liver function. If untreated, fibrosis can advance to cirrhosis, hepatocellular carcinoma, or liver failure (Pellicoro et al., 2014). The severity of fibrosis is closely correlated with liver-related outcomes and overall mortality (Angulo et al., 2015). A better understanding of the processes leading to fibrosis is therefore essential to improve our current in vitro models.

The pathology of liver fibrosis has been described in the liver fibrosis AOP No. 38 (Horvat et al., 2017). Protein alkylation (MIE) induced by drugs or viral infections, causes hepatocellular death or injury (KE1). Damaged hepatocytes activate Kupffer cells (KCs), the liver's resident macrophages, through the release of reactive oxygen species, cytokines and damage-associated molecular patterns (KE2). Upon activation, KCs become the primary source of transforming growth factor beta 1 (TGF-β1), the most pro-fibrogenic cytokine, and other inflammatory cytokines (KE3). Excessive release of TGF-β1 stimulates the activation of hepatic stellate cells (HSCs), which transition from a quiescent vitamin A-storing phenotype to a proliferative, contractile myofibroblast-like phenotype (KE4). Activated HSC secret extracellular matrix (ECM) components, including collagen type I and fibronectin, driving fibrosis progression. Excessive accumulation of collagen and other ECM components leads to the replacement of liver tissue by connective tissue and marks key event 5 (KE5), which ultimately leads to the adverse event, liver fibrosis (Horvat et al., 2017).

While advanced MPS models exist for studying fibrosis, they are not designed to specifically address the key events described in the AOP. This limits their usefulness for the development of quantitative AOPs and makes it difficult to define and measure parameters for in silico modelling (Kanabekova et al., 2022; Kostrzewski et al., 2021). Furthermore, existing MPS models often employ direct cell-cell contact between the different cell types, which hinders the analysis of individual cellular responses (Bircsak et al., 2021; Cho et al., 2021). Although techniques, such as single-cell sequencing can be used to investigate cell-type specific responses, they are costly and often require outsourcing. In addition, many MPS rely on complex fabrication methods, external tubing and pumps, which complicate scalability, throughput and introduce potential issues regarding drug adsorption (Dalsbecker et al., 2022). To address these challenges, we developed a simplified in vitro liver fibrosis model using the commercially available Akura™ Twin platform. The Akura™ Twin platform is a specially designed 384-well microplate with interconnected wells. The wells can host 3D-cultures such as spheroids or organoids (microtissues: MTs) and the platform allows gravity-driven flow between MTs without the need for external pumps or tubing. This design minimizes compound adsorption and enables simultaneous testing of 168 conditions, making it a suitable tool for high-throughput studies.

To model liver fibrosis, we incorporated the three key cell types described in the AOP: hepatocytes, Kupffer cells, and hepatic stellate cells (Horvat et al., 2017). HepaRG cells were chosen as hepatocyte surrogates due to their metabolic similarity to primary hepatocytes, while THP-1 monocyte-derived macrophages served as Kupffer cell surrogates, and hTERT-immortalized primary HSCs were used as hepatic stellate cell surrogates (Prestigiacomo et al., 2017; Rubin et al., 2015; Schnabl et al., 2002; Wu et al., 2016). Human cell lines were chosen to establish a robust and reproducible model, since primary cells often exhibit significant donor-to-donor variation (Josse et al., 2012) and may be difficult to obtain for high-throughput studies.

Striking a balance between physiological relevance and experimental complexity, we tested two experimental setups. The first consisted of HepaRG MTs connected by shared medium with HSC MTs, forming the baseline fibrosis model. The second setup incorporated immune cells by co-culturing THP-1 monocyte-derived macrophages within the HepaRG MTs while maintaining contact with HSC MTs. Liver cells were challenged with TGF-β1, methotrexate (MTX) or acetaminophen (APAP). TGF-β1, a well-established pro-fibrotic factor, was used as a positive control (Bonanini et al., 2025). MTX, an anti-rheumatic drug reported to induce liver fibrosis in some patients and in vitro, was tested as a fibrotic test compound (Cheng & Rademaker, 2018; Lertnawapan et al., 2023; MacDonald & Burden, 2005; Mikkelsen et al., 2011). Finally, APAP, a well-characterized hepatotoxic compound, was included to model acute hepatotoxicity that is not associated with subsequent fibrosis in the clinic (Jaeschke et al., 2020; Yoon et al., 2016).

Here, we successfully developed a scalable in vitro liver fibrosis model capable of studying the key events involved in hepatic fibrosis. By implementing the Akura™ Twin platform and combining several relevant human liver cell types, we could link the five key events defined in the liver AOP to specific and quantifiable markers. Hence, this model represents a valuable tool for studying liver fibrosis and to generate quantitative AOP data that can be used for dose-response and time-course predictions supporting regulatory decision-making.

2. Materials and methods

2.1. Cell culture

All procedures were performed under sterile conditions following standard laboratory procedures. Cells were cultured at 37°C with 5 % CO_2 in a humidified incubator.

HepaRG cells (Biopredic International, Saint Grégoire, France, HPR101) were seeded at 1×10^5 undifferentiated cells/cm^2 in basal medium (Biopredic International, Saint Grégoire, France, MIL700C) supplemented with growth factors (Biopredic International, Saint Grégoire, France, ADD710C). After 14 days, the growth medium was replaced with a 50:50 mix of growth and differentiation supplements (Biopredic International, Saint Grégoire, France, ADD720C) for four days, followed by differentiation medium alone for an additional 10 days. HepaRG cells were used at passages below 20 and passaged with Trypsin-EDTA (Sigma, Taufkirchen, Germany, 59417C-mL).

hTERT-HSC cells were kindly provided by Dr. Bernd Schnabl (UC, San Diego, CA 92103, USA) and cultured in Dulbecco's Modified Eagle's Medium (DMEM) High Glucose (Fisher Scientific, Reinach, Switzerland, 41965062), supplemented with 10 % fetal bovine serum (FBS, Fisher Scientific, Reinach, Switzerland, 10270–106) and 1 % penicillin and streptomycin (P/S, Sigma, Taufkirchen, Germany, P4333–mL). To prevent spontaneous activation, hTERT-HSC cells were used at low passages (<12) and passaged using Trypsin-EDTA.

THP-1 cells (CLS, Eppelheim, Germany, 300356) were maintained in suspension at 1.5–10 $\times$ 10^5 cells/mL in Roswell Park Memorial Institute 1640 medium (RPMI, Bioconcept, Allschwil, Switzerland, 1–41F50-I), supplemented with 10 % FBS and 1 % P/S. The culture was passaged by diluting the suspension or replacing the complete medium every other day.

2.2. Microtissue preparation

THP-1 cells were differentiated into monocyte-derived macrophages by seeding 8×10^4 cells/cm^2 in a T25 flask with RPMI medium supplemented with 10 % FBS, 1 % P/S, and 100 ng/mL phorbol 12-myristate 13-acetate (PMA, Fisher Scientific, Reinach, Switzerland, P1585–1MG). After 48 h, the medium was replaced with PMA-free RPMI medium containing 10 % FBS and 1 % P/S. Cells were allowed to rest for an additional 24 h before use.

MT aggregation was performed in Akura™ 96 Plates (InSphero, Schlieren, Switzerland, CS-PB15). Wells were pre-wetted with maintenance medium consisting of William's E Medium

(ThermoFisherScientific, Reinach, Switzerland, 32551087) supplemented with 1X Insulin-Transferrin-Sodium Selenite (ITS, Sigma, Taufkirchen, Germany, 11074547001), 100 nM dexamethasone (Sigma, Taufkirchen, Germany, D1756) and 1 % P/S. Differentiated HepaRG and hTERT-HSC cells were detached using Trypsin-EDTA, while differentiated THP-1 were detached using Accumax (FisherScientific, Reinach, Switzerland, 00–4666–56). Each cell type was individually resuspended in maintenance medium supplemented with 20 % FBS and cell numbers were counted. Three distinct MT types were prepared, namely HepaRG MTs, HepaRG + THP-1 MTs and HSC MTs. Cell composition is detailed in Table 1. Cell suspensions were seeded at 70 μL per well, followed by centrifugation at 250 x g for 2 min. Plates were incubated in a humidified incubator for 4 days, with the first 24 h on an Akura™ Tilting stand (30°, InSphero, Schlieren, Switzerland, CS-AG11). After 4 days, the medium was replaced by FBS-free maintenance medium.

2.3. Microtissue transfer and treatment

The Akura™ Twin microplate (InSphero, Schlieren, Switzerland, CS-PE13) was pre-wetted by adding 80 μL pre-warmed H_2O to the alpha well. After 3 min of liquid equilibration, the plate was centrifuged at 500 x g for 2 min and incubated overnight in a humidified incubator. The following day, water was removed by aspirating 80 μL from the alpha well followed by the beta well within 5 s. 100 μL of maintenance medium was then added to each alpha well. After another 3 min of liquid equilibration, the plate was centrifuged at 500 x g for 2 min. Before MT transfer, the medium was removed as described above.

MTs were washed twice with maintenance medium before transfer. To prevent MTs from adhering to plastic surfaces, pipette tips were coated with FBS. MTs were collected in 40 μL of maintenance medium and gently dispensed into the designated wells of the Akura™ Twin microplate. To minimize cross-contamination of loose THP-1 cells, HSC MTs were transferred first to the beta wells followed by HepaRG + THP-1 MTs to the alpha wells. After transfer, maintenance medium was removed as previously described and 100 μL of fresh maintenance medium was added to beta wells.

After 24 h of incubation, treatments were initiated. TGF-β1 1 ng/mL (Sigma, Taufkirchen, Germany, T7039–1UG) was used as positive control for stellate cell activation, MTX 30 μM (Sigma, Taufkirchen, Germany, M8407–100MG) was employed as a fibrotic test compound, while APAP 2 mM (Sigma, Taufkirchen, Germany, A5000) was utilized as a non-fibrotic hepatotoxicant. Compounds were diluted in maintenance medium and 100 μL per beta well was added. Treatment was carried for 10 days and refreshed on days 3, 5 and 7. To generate gravity-based flow, an All-in-One Tilting device was used with the following settings: tilt angle ± 20°, motion time 10 s, pause at (P/N = ± 20°) for 1 min, pause at (H = ± 0°) for 0 min, and timer set to 0 s (continuous operation).

2.4. Bioenzymatic sensor measurements

Glucose and lactate levels were measured in the supernatant on days 3, 7 and 10 using the B.LV5 biosensor (Jobst Technologies, Freiburg, Germany, 1.00101.002) connected to the SIX Biosensor Transmitter (Jobst Technologies, Freiburg, Germany). For each measurement, 50 μL of supernatant was injected into the sensor unit and allowed to equilibrate for 20 s before data acquisition for 60 s using the bioMON software (Version 4.16.0).

Table 1
Cell numbers and composition per MT.

	Number of cells per MT		
	HepaRG	THP-1	hTERT-HSC
HepaRG MTs	2'000	-	-
HepaRG + THP−1 MTs	1'500	500	-
HSC MTs	-	-	2'000

2.5. Enzyme-Linked Immunosorbent Assay (ELISA)

The concentration of albumin (Bethyl Laboratories, Montgomery, TX, USA, E80–129), connective tissue growth factor (CTGF, Bio Techne AG, Zug, Switzerland, DY9190–05), Pro-Collagen 1A1 (Bio Techne AG, Zug, Switzerland, DY6220–05) and plasminogen activator inhibitor-1 (PAI-1, Bio Techne AG, Zug, Switzerland, DY1786) was measured in cell culture supernatant on days 3, 7 and 10. All ELISA assays were performed in high-binding flat-bottom plates (Greiner-Bio One, Kremsmünster, Austria, 655 061), according to manufacturers' instructions. Absorbance at 450 nm was measured using the FlexStation 3.

2.6. Urea release

Urea release was quantified in the supernatant after 3, 7 and 10 days using the Urea Assay Kit (Sigma, Taufkirchen, Germany, MAK006). Volumes were adjusted for a 384 well format (Table S1). For each well, 12.5 μL of the appropriate Reaction Mix was prepared. Samples were diluted 1:5 in Urea Assay Buffer. Two standard curves were prepared, one without and one spiked with 2 mM APAP. 12.5 μL diluted cell supernatant or standards were added and mixed thoroughly using a horizontal shaker. The reaction was incubated for 60 min at 37°C, protected from light. Absorbance was measured at 570 nm using the FlexStation 3. Calculations were performed according to manufacturer's instructions.

2.7. Immunofluorescence staining

Unless otherwise stated, compounds were obtained from Sigma (Taufkirchen, Germany). Immunofluorescence staining was performed on MTs collected on day 10. For each experimental condition and MT composition, 1–4 MTs were collected and washed in PBS containing calcium and magnesium. The MTs were fixed for 1 h in 4 % paraformaldehyde (PFA), followed by permeabilization for 24 h at 4°C using 0.5 % Triton X-100. The MTs were then blocked with 3 % bovine serum albumin (BSA) and 0.1 % Triton X-100 at 4°C overnight. Primary antibodies (diluted as outlined in Table 2) were prepared in 1 % BSA and 0.1 % Triton X-100. HepaRG and HepaRG + THP-1 MTs were stained for albumin, while HSC MTs were stained for αSMA, fibronectin and f-actin (phalloidin). The MTs were incubated with primary antibody overnight at 4°C. After incubation, the samples were washed with 0.1 % Triton X-100 and incubated overnight at 4°C with secondary antibodies (diluted as indicated in Table 2), diluted in 1 % BSA and 0.1 % Triton X-100. The MTs were washed again and counter-stained with DAPI for 1 h at room temperature before imaging. Images were acquired using an Olympus Fluoview FV3000 confocal microscope. Image analysis was performed with ImageJ and CellProfiler (Software 4.2.1).

Table 2
Antibodies and phalloidin used for immunofluorescence staining.

Protein of Interest	Primary Antibody	Secondary Antibody
Albumin	Rabbit monoclonal antibody (Abcam, Cambridge, United Kingdom, ab207327) / 1:800	Goat anti-rabbit Alexafluor 546 (FisherScientific, Reinach, Switzerland, A−11071) / 1:1000
αSMA	Mouse polyclonal antibody (Sigma, Taufkirchen, Germany, A5228) / 1:400	Goat anti-mouse Alexafluor 488 (FisherScientific, Reinach, Switzerland, A−11017) / 1:1000
Fibronectin	Rabbit polyclonal antibody (Agilent, Waldbronn, Germany, A0245) / 1:400	Goat anti-rabbit Alexafluor 647 (FisherScientific, Reinach, Switzerland, A−21245) / 1:1000
Phalloidin	TRITC-labelled (Sigma, Taufkirchen, Germany, P1951) / 1:1000	

2.8. Gene expression analysis

On days 7 and 10, MTs were collected for mRNA isolation. For each experimental condition and MT composition, 2–6 MTs were collected. mRNA was isolated using a standard TRIzol extraction procedure with glycogen (FisherScientific, Reinach, Switzerland, LT-02241) from MTs lysed with QIAzol Lysis Reagent (Qiagen, Basel, Switzerland, 79306). Reverse transcription was performed using M-MLV Reverse transcriptase (Promega, Dübendorf, Switzerland, M1705) and oligo dT (Promega, Dübendorf, Switzerland, C110B-C). Real-time PCR was carried out using GoTaq® Probe qPCR Master Mix (Promega, Dübendorf, Switzerland, A6102) and TaqMan probes of selected genes (Table 3). The q-RT-PCR Program was as follows: the reaction was initiated at 95°C for 2 min, followed by 40 cycles of 15 s at 95°C and 1 min at 60°C. Ct values were generated using the LightCycler® 480 System. Beta-2-Microglobulin (B2M) was used as the internal standard for normalization. Data are expressed as fold change.

2.9. Statistical analysis

All data were analyzed using GraphPad Prism 10 (Version 10.4.1; GraphPad Software). Ordinary one-way ANOVA followed by Dunnett's multiple comparisons test was employed to assess statistical differences among treatment groups against a single control for semi-quantitative or normalized analyses (e.g. Mean Fluorescence Intensity, qPCR). In cases where only a single experimental setup was analyzed, an unpaired Student's *t*-test was performed. For quantitative endpoints involving two independent variables (setup and treatment), an ordinary two-way ANOVA followed by Tukey's multiple comparisons test was performed to evaluate interaction and main effects. A p-value of ≤ 0.05 was considered statistically significant.

3. Results

3.1. Treatments affected cellular metabolism as reflected by changes in lactate production and glucose consumption

Lactate and glucose levels in the supernatant were monitored over 10 days as indicators of cellular metabolism using the B.LV5 biosensor from Jobst. As depicted in Fig. 1A, lactate production by HepaRG MTs connected with HSC MTs remained unaffected by any treatment after 3 days of exposure. In the control group, lactate production increased from 1.0 to 1.9 µg/day over 10 days. The addition of THP-1 cells markedly increased lactate release under both untreated and TGF-β1 treated conditions, which displayed a time dependent increase in lactate production with medians of 2.1, 7.1 and 20.0 µg/day at 3, 7 and 10 days respectively. Consistent with toxicity, treatment with MTX or APAP significantly reduced lactate production from day 7 onward. The most pronounced reduction was observed in APAP-treated cultures at day 10, with a rate of 0.8 µg/day.

Similar to the lactate measurements, glucose consumption was relatively unchanged in untreated HepaRG MTs connected with HSC MTs over the measurement period with values ranging from 9.1 to 13.8 µg/day (Fig. 1B). In the presence of THP-1, glucose consumption significantly increased over time in the untreated and TGF-β1-treated conditions, reaching a median of 30.5 µg/day by day 10. In contrast, MTX and APAP showed similar glucose consumption levels over 10 days.

Overall, HepaRG//HSC cultures maintained cellular metabolism over 10 days for all treatments. HepaRG + THP-1//HSC cultures showed an increased cellular metabolism in the untreated and TGF-β1 treated conditions, which reflects the increased number of THP-1 cells over time (Fig. S1). Outgrowing cells were albumin negative, further supporting that the increased cellular metabolism can be attributed to the THP-1 cells (Fig. S2).

Table 3
TaqMan probes of selected genes obtained from FisherScientific (Reinach, Switzerland).

Gene of interest	Abbreviation	Ref. Nr.
Actin alpha 2, smooth muscle	ACTA2	Hs00909449_m1
Arachidonate 5-lipoxygenase-activating protein	ALOX5AP	Hs00233463_m1
Beta−2-Microglobulin	B2M	Hs00187842_m1
Collagen 1 alpha 1	COL1A1	Hs00164004_m1
Collagen 3 alpha 1	COL3A1	Hs00943809_m1
Fibronectin 1	FN1	Hs00415006_m1
Transforming growth factor beta 1	TGF-β1	Hs00998133_m1
Triggering receptor expressed on myeloid cells 2	TREM2	Hs00219132_m1

3.2. Hepatocellular damage is observed upon stimuli with TGF-β1, MTX and APAP

The first key event in the liver fibrosis AOP is hepatocellular death or injury. To assess hepatocyte health, albumin release was measured in the supernatant using ELISA (Fig. 2A). Both HepaRG and HepaRG + THP-1 MTs maintained albumin secretion over 10 days.

Treatment with TGF-β1 and APAP led to acute hepatocellular damage evidenced by the reduction in albumin production in HepaRG and HepaRG + THP-1 MTs from day 3 onwards. On the other hand, MTX showed delayed toxicity and a decreased albumin release only from day 7. Notably, incorporation of THP-1 cells slightly increased albumin secretion for all conditions.

As an additional biomarker of hepatocellular function, urea levels were measured in the supernatant after 3, 7 and 10 days (Fig. 2B). In HepaRG//HSC cultures, neither TGF-β1 nor MTX significantly affected urea production. Urea levels were maintained over time with values ranging from 18.5 to 40.5 pg/h/HepaRG. In contrast, APAP treatment significantly reduced the urea levels by 25–60 %. Unexpectedly, the incorporation of THP-1 resulted in significantly elevated urea production across all treatments by 2–3-fold. Moreover, the HepaRG + THP-1 MTs exhibited increased sensitivity to MTX and APAP treatment compared to the cultures without THP-1 cells, resulting in a strong reduction of urea release starting from day 7.

To further validate these findings, the intracellular expression of albumin was analyzed by immunofluorescence staining after 10 days (Fig. 3A). Consistent with the observed reduction in secreted albumin levels, exposure to TGF-β1 or APAP resulted in a significant loss of albumin expression across all experimental setups (Fig. 3B). In contrast, MTX treatment had no apparent effect on intracellular albumin expression.

3.3. Activation of THP-1 is triggered by TGF-β1 and suppressed by APAP treatment

During the development of fibrosis, following hepatocyte death or injury, Kupffer cells are activated (KE2). To assess their activation, the mRNA expression levels of ALOX5AP (Fig. 4A) and TREM2 (Fig. 4B) in THP-1 were measured at 7 and 10 days. TGF-β1 treatment significantly upregulated both markers, with ALOX5AP expression increasing by more than 7-fold and TREM2 expression increasing by 2-fold at both timepoints. In contrast, APAP led to a consistent downregulation of both genes. MTX treatment did not directly activate THP-1 and hence had no significant effect on the expression levels of either marker. The observed variability in gene expression levels is most likely attributed to general biological variability. To make sure that ALOX5AP and TREM2 mRNA levels are derived from THP-1 cells and not from the HepaRG, we also assessed the gene expression levels of ALOX5AP and TREM2 in HepaRG MTs without THP-1 cells. For all conditions, the measured Ct values were above the cut-off value of 35 or undetectable. We further assessed the release of the acute phase cytokine IL-6 in the supernatant of

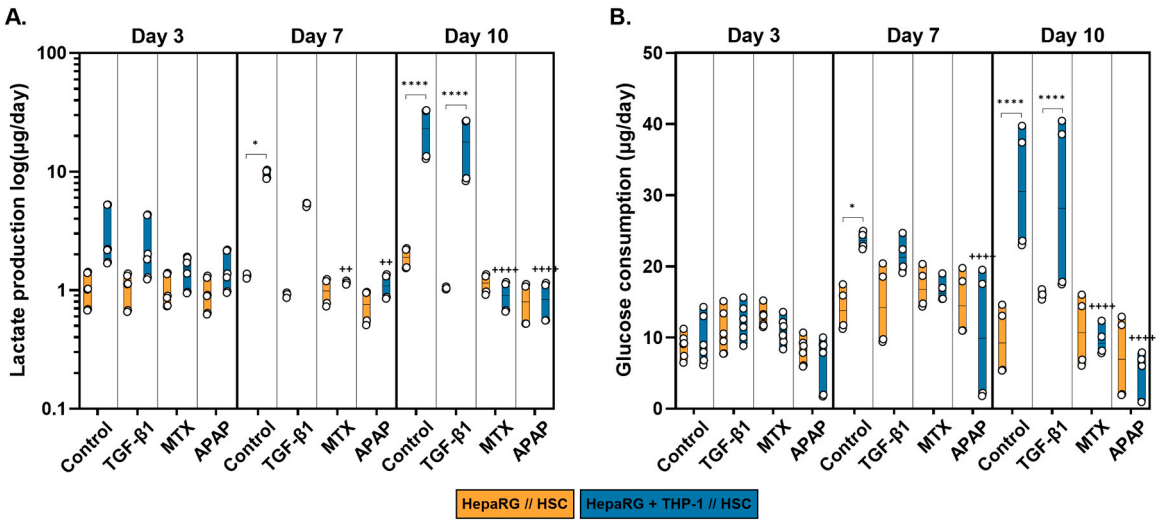

Fig. 1. Lactate production and glucose consumption over 10 days. HepaRG MTs connected with HSC MTs (orange) and HepaRG + THP-1 MTs connected with HSC MTs (blue), were exposed to TGF-β1, MTX, or APAP for 10 days. Lactate production (A) and glucose consumption (B) were measured in the culture supernatant on days 3, 7, and 10 using the B.LV5 biosensor (Jobst). Metabolic rates are expressed in µg/day. For better visualization of the single data points, lactate production was plotted as log10(µg/day). Floating bars represent median ± min max. Statistical analysis based on ordinary two-way ANOVA, followed by Tukey's multiple comparisons test, with */+ , $p \leq 0.05$; **/+ +, $p \leq 0.01$; ***/+ ++ , $p \leq 0.001$; ****/+ ++ +, $p \leq 0.0001$. * represents comparisons between setups, + represents comparison to HepaRG + THP-1//HSC controls of the respective timepoint. N = 3 – 4 (3 – 4 independent biological replicates with 1 – 2 technical replicates).

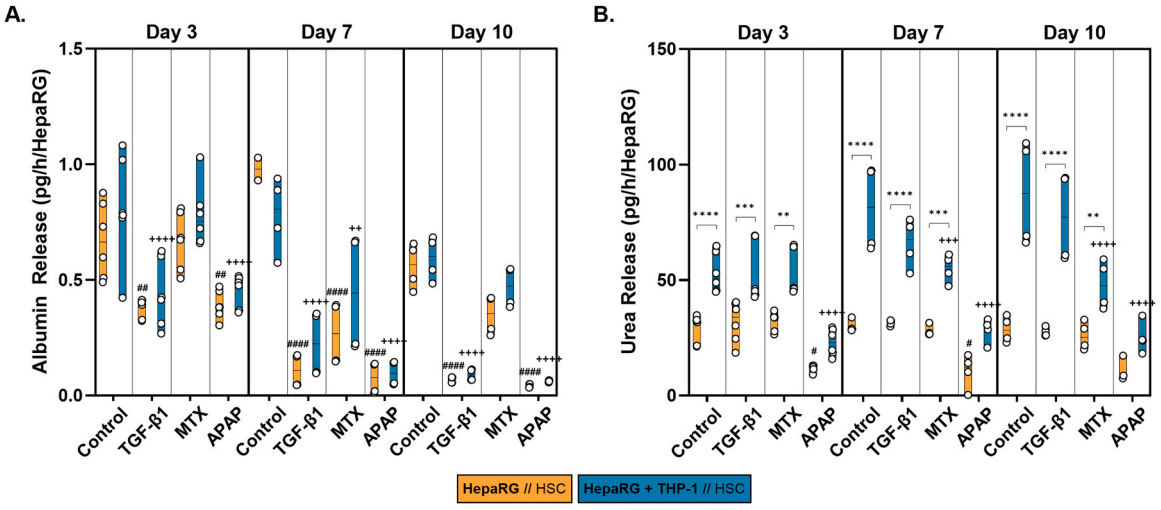

Fig. 2. Effects of TGF-β1, MTX or APAP on HepaRG cells health and functionality. HepaRG MTs connected with HSC MTs (orange) and HepaRG + THP-1 MTs connected with HSC MTs (blue), were exposed to TGF-β1, MTX, or APAP for 10 days. Albumin (A) and urea (B) release were measured in the supernatant after 3, 7 and 10 days. Floating bars represent median ± min max. Statistical analysis based on ordinary two-way ANOVA, followed by Tukey's multiple comparisons test, with */#/+ , $p \leq 0.05$; **/##/+ +, $p \leq 0.01$; ***/###/+ ++ , $p \leq 0.001$; ****/####/+ ++ +, $p \leq 0.0001$. * represents comparisons between setups, # represents comparison to HepaRG//HSC controls and + represents comparison to HepaRG + THP-1//HSC controls of the respective timepoint. N = 3 – 4 (3 – 4 independent biological replicates with 1 – 2 technical replicates).

HepaRG + THP-1//HSC cultures and observed increased levels after 3 and 7 days following TGF-β1 treatment (Fig. S5).

3.4. TGF-β1 increased the release of PAI-1 in the supernatant

Activation of the Kupffer cells triggers the third key event (KE3): the secretion of the pro-fibrogenic cytokine TGF-β1. To investigate this, we measured TGF-β1 mRNA expression in THP-1 cells and the concentration of a downstream marker (PAI-1) in the supernatant. Consistent with the induction of THP-1 activation markers ALOX5AP and TREM2, a significant 1.9-fold upregulation of TGF-β1 mRNA was observed in TGF-β1-treated HepaRG + THP-1 MTs on day 7 (Fig. 5A). The effect of TGF-β1-treatment on TGF-β1 seemed transient as its mRNA expression returned to baseline at 10 days. MTX and APAP significantly suppressed TGF-β1 expression (2.9-fold and 2.1-fold downregulation, respectively).

As a downstream effect of TGF-β1, PAI-1 secretion increased significantly in response to TGF-β1 treatment across all setups and at all tested time points (Fig. 5B). PAI-1 secretion peaked in THP-1 containing cultures (1.5 ± 0.3 pg/day) from day 7 onwards, significantly surpassing HepaRG//HSC cultures (0.7 ± 0.4 pg/day). These results suggest that TGF-β1 activates THP-1 cells towards an anti-inflammatory phenotype. Contrarily, MTX and APAP treatments did not cause changes with respect to the corresponding untreated cells.

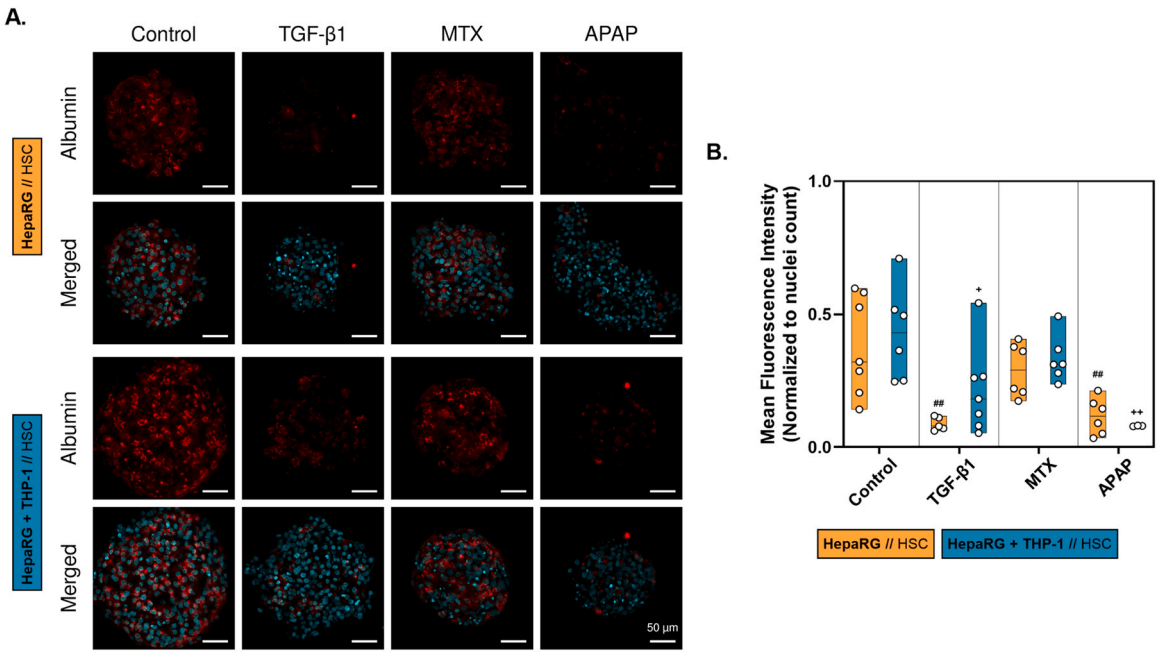

Fig. 3. Albumin expression in HepaRG cells following treatment with TGF-β1, MTX or APAP. HepaRG MTs and HepaRG + THP-1 MTs in contact with HSC MTs, were treated with TGF-β1, MTX, or APAP for 10 days. After treatment, HepaRG MTs and HepaRG + THP-1 MTs were fixed and stained for albumin (red) and counter-stained with DAPI (blue) (A). Scale bar = 50 µm. Mean fluorescence intensity was quantified and normalized to nuclei count (B). Floating bars represent median ± min max. Statistical analysis was performed using ordinary one-way ANOVA, followed by Dunnett's multiple comparisons test, with #/+ , $p \leq 0.05$; ##/+ +, $p \leq 0.01$. # represents comparison to HepaRG//HSC controls and + represents comparison to HepaRG + THP-1//HSC controls. N = 3 (3 independent biological replicates with 1 – 3 technical replicates).

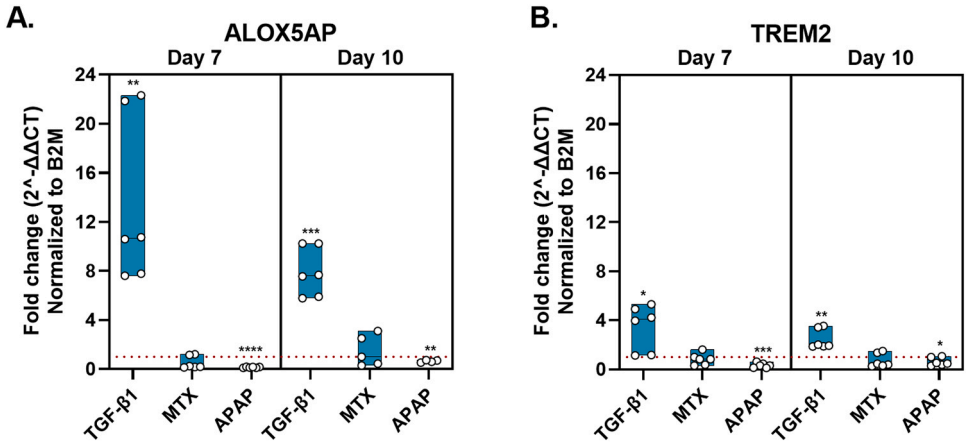

Fig. 4. Activation of THP-1 by TGF-β1 treatment. HepaRG + THP-1 MTs in contact with HSC MTs were exposed to TGF-β1, MTX or APAP for 10 days. Q-RT-PCR was performed on days 7 and 10 to assess mRNA expression levels of ALOX5AP (A) and TREM2 (B). Red dashed lines indicate baseline expression of untreated control. Floating bars represent median ± min max. Statistical analysis based on Student's unpaired *t*-test, with *, $p \leq 0.05$; **, $p \leq 0.01$; ***, $p \leq 0.001$. * *represents comparison to HepaRG + THP-1//HSC controls of the respective timepoint.* N = 3 (3 independent biological replicates with 2 technical replicates).

3.5. Activation of HSC is observed upon treatment with TGF-β1

The next step in the AOP cascade is the activation of the hepatic stellate cells (KE4). Activation was determined by measuring transcript and protein amounts of the HSC activation marker alpha smooth muscle actin (αSMA, Gene: ACTA2) and the ECM marker fibronectin (Gene: FN1). Treatment with TGF-β1 led to a significant upregulation of ACTA2 mRNA in both culture conditions after 7 and 10 days (Fig. 6A). Specifically, fold increases of 5.0 and 3.9 were observed on day 7, and 3.0 and 1.8 on day 10 for HepaRG//HSC and HepaRG + THP-1//HSC cultures, respectively. APAP treatment resulted in a 2.3-fold downregulation of ACTA2 in HepaRG//HSC cultures after 10 days, while MTX had no significant effect. Similarly, FN1 expression was upregulated by TGF-β1 with 5.1- and 2.1-fold increases on day 7 and 2.6- and 1.8-fold increases on day 10 for the same respective setups (Fig. 6B). Neither MTX nor APAP significantly altered FN1 transcriptional levels. On day 7, high variability was observed for both markers in TGF-β1- and MTX-treated conditions. This variation is potentially attributed to spontaneous activation of HSCs impairing baseline activation levels. After 10 days in culture, these effects seem to stabilize, resulting in reduced variability.

To confirm HSC activation at the protein level, cells were stained for f-actin (phalloidin), αSMA, and fibronectin after 10 days in culture (Fig. 7A). TGF-β1 treatment significantly increased fibronectin (Fig. 7B) and f-actin (Fig. 7C) expression across all experimental setups, while MTX and APAP showed no effect. For αSMA, we quantified the cytoskeletal features using ImageJ deconvolution followed by stress fiber

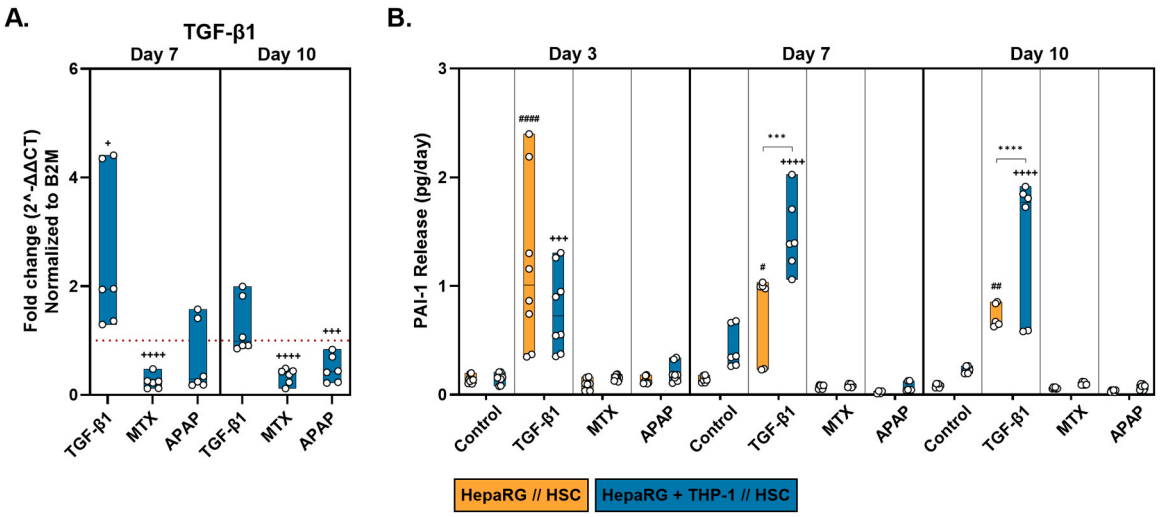

Fig. 5. TGF-β1 treatment increases TGF-β1 expression in THP-1 and the secretion of downstream marker PAI-1. HepaRG MTs and HepaRG + THP-1 MTs in contact with HSC MTs were exposed to TGF-β1, MTX or APAP for 10 days. Q-RT-PCR was performed after 7 and 10 days to detect mRNA expression levels of TGF-β1 in HepaRG + THP-1 MTs (A). Red dashed lines represent baseline expression of untreated control. Levels of PAI-1 were measured in the supernatant after 3, 7 and 10 days (B). Floating bars represent median ± min max. Statistical analysis based on unpaired Student's *t*-test (A) or ordinary two-way ANOVA, followed by Tukey's multiple comparisons test (B), with $^{*/\#/+}$, $p \leq 0.05$; $^{**/\#\#/++}$, $p \leq 0.01$; $^{***/\#\#\#/+++}$, $p \leq 0.001$; $^{****/\#\#\#\#/++++}$, $p \leq 0.0001$. * represents comparisons between setups, $^{\#}$ represents comparison to HepaRG//HSC controls and $^{+}$ represents comparison to HepaRG + THP-1//HSC controls of the respective timepoint. N = 3 – 4 (3 – 4 independent biological replicates with 2 technical replicates).

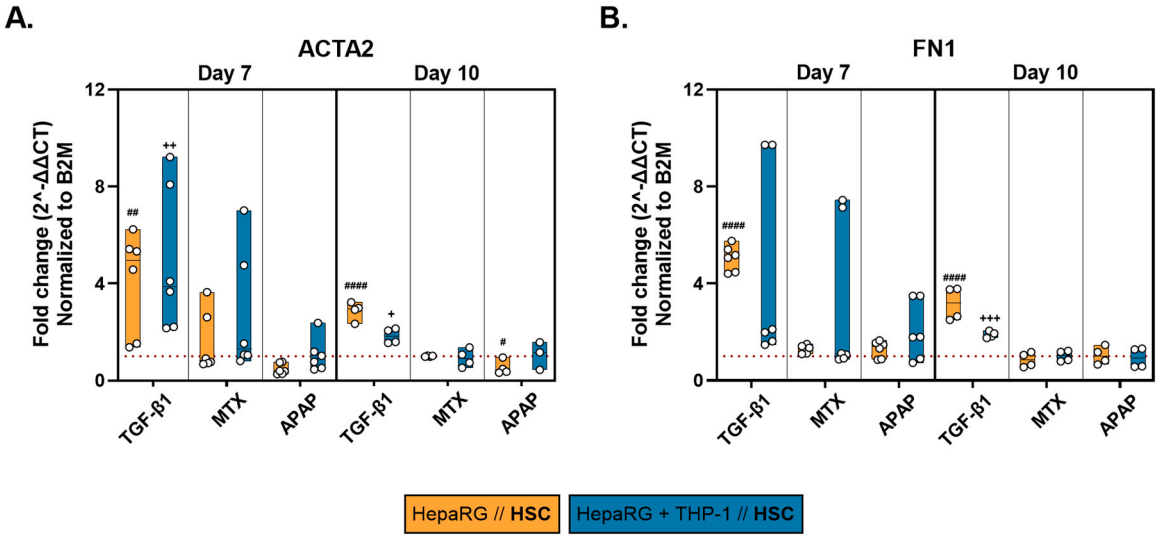

Fig. 6. TGF-β1 increases activation marker ACTA2 and ECM marker FN1. HepaRG MTs or HepaRG + THP-1 MTs in contact with HSC MTs were exposed to TGF-β1, MTX or APAP for 10 days. Q-RT-PCR was performed after 7 and 10 days to assess mRNA expression levels of ACTA2 (A) and FN1 (B). Red dashed lines represent baseline expression of untreated control. Floating bars represent median ± min max. Statistical analysis based on ordinary one-way ANOVA followed by Dunnett's multiple comparisons test, with $^{\#/+}$, $p \leq 0.05$; $^{\#\#/++}$, $p \leq 0.01$; $^{\#\#\#/+++}$, $p \leq 0.001$; $^{\#\#\#\#/++++}$, $p \leq 0.0001$. $^{\#}$ represents comparison to HepaRG//HSC controls and $^{+}$ represents comparison to HepaRG + THP-1//HSC controls of the respective timepoint. N = 3 (3 independent biological replicates with 1 – 2 technical replicates).

quantification in CellProfiler This allowed for specific assessment of aSMA-positive fiber structures indicative of HSC activation (Fig. 7D). The quantitative analysis revealed a significant increase in fiber count per microtissue following TGF-β1 treatment. However, some variability was observed and a subset of spheroids in both control groups exhibited levels of activation comparable to TGF-β1-treated groups, possibly due to spontaneous HSC activation. Neither MTX nor APAP increased fiber numbers. These results align with the transcriptional data, confirming selective activation of HSCs by TGF-β1.

3.6. TGF-β1 increases Pro-Collagen 1A1 and CTGF secretion

The final key event (KE5) described in the liver fibrosis AOP involves excessive collagen accumulation and changes in ECM composition. To investigate KE5, we measured mRNA expression of COL1A1 and COL3A1. TGF-β1 increased COL1A1 levels in all models on both timepoints (Fig. 8A). On day 10, for example, fold changes of 5.2- and 1.9-fold for HepaRG//HSC and THP-1 containing cultures, were observed. Neither MTX nor APAP affected COL1A1 expression. For COL3A1 (Fig. 8B), TGF-β1 induced a moderate increase in HepaRG//HSC up to 1.7-fold on day 10. APAP suppressed the expression of COL3A1, while MTX showed no clear induction or inhibition.

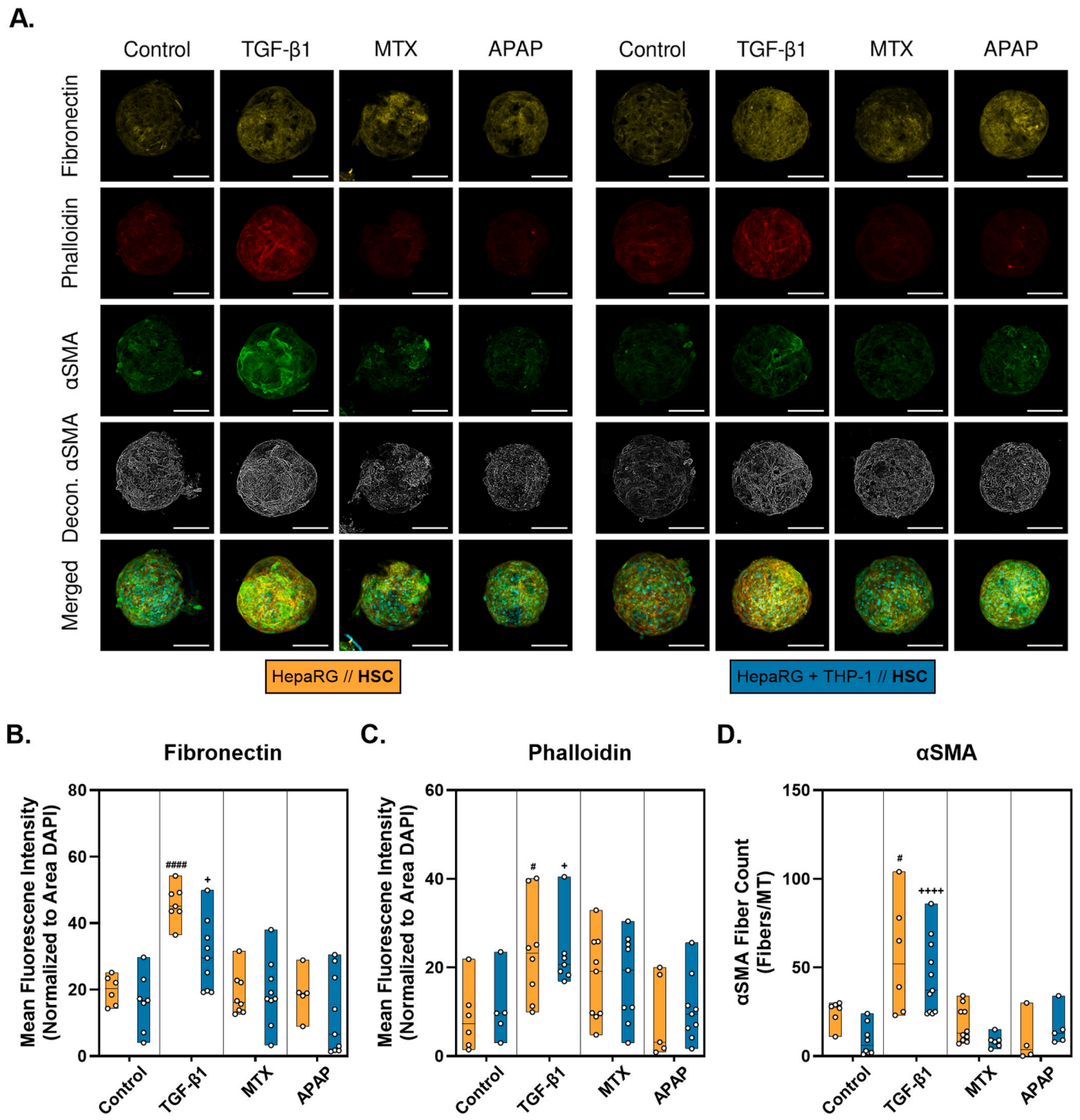

Fig. 7. TGF-β1 induces HSC activation. HepaRG MTs or HepaRG + THP-1 MTs connected with HSC MTs were treated with TGF-β1, MTX, or APAP for 10 days. HSC MTs were fixed and stained for fibronectin (yellow), phalloidin (red), αSMA (green), and counterstained with DAPI (blue) (A). Deconvolved images of αSMA are shown in white. Scale bar = 100 μm. Mean fluorescence intensity of fibronectin (B) and phalloidin (C) was quantified and normalized to area DAPI. Single αSMA fibers were detected using CellProfiler and normalized to the number of MTs per image (D). Floating bars show median ± min to max (B, C, D). Statistical analysis was performed using ordinary one-way ANOVA, followed by Dunnett's multiple comparisons test, with $^{\#/+}$, $p \leq 0.05$; $^{\#\#/++}$, $p \leq 0.01$; $^{\#\#\#/+++}$, $p \leq 0.001$; $^{\#\#\#\#/++++}$, $p \leq 0.0001$. $^{\#}$ represents comparison to HepaRG//HSC controls and $^{+}$ represents comparison to HepaRG + THP-1//HSC controls. N = 3 (3 independent biological replicates with 1 – 3 technical replicates).

To assess ECM remodeling at the protein level, we quantified Pro-Collagen 1A1 and CTGF in the culture supernatant. Despite inter-replicate variability in absolute values, treatment-to-control ratios were consistent and used for normalization. After 7 days, TGF-β1 significantly increased Pro-Collagen 1A1 secretion (1.8- and 1.5-fold without and with THP-1 cells) (Fig. 8C). APAP showed the opposite trend. After 10 days, TGF-β1 maintained elevated Pro-Collagen 1A1 secretion in HepaRG//HSC cultures (2.0-fold), while APAP decreased levels by 4.8-fold in HepaRG//HSC and 4.5-fold in HepaRG + THP-1// HSC cultures.

Interestingly, CTGF exhibited an earlier response than Pro-Collagen 1A1 (Fig. 8D). TGF-β1 significantly increased CTGF secretion across all setups after 3 and 7 days (3.7-, 2.6-fold and 2.6-, 2.5-fold increases, respectively). MTX and APAP significantly suppressed CTGF levels in

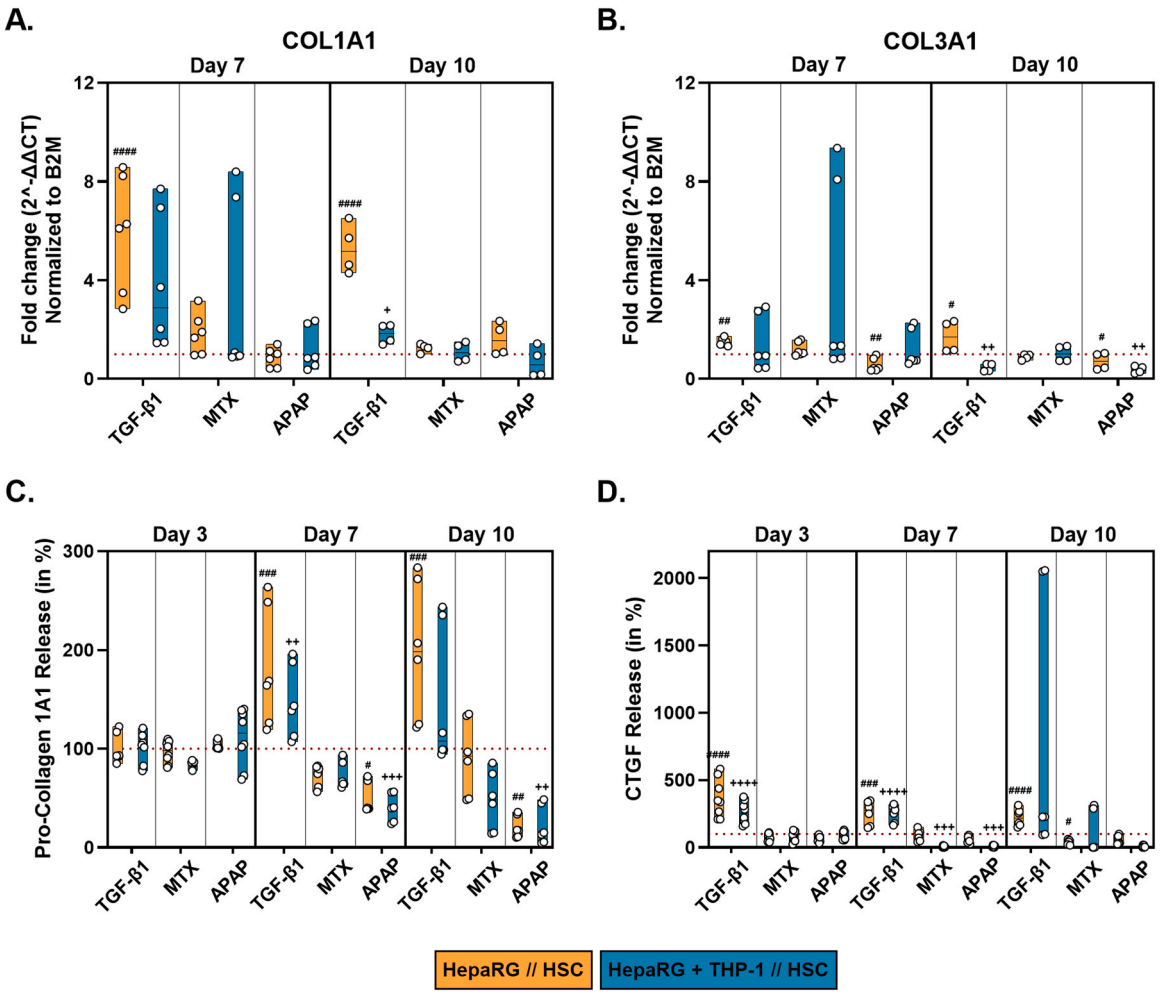

Fig. 8. TGF-β1 induces ECM remodeling. HepaRG MTs or HepaRG + THP-1 MTs connected with HSC MTs were exposed to TGF-β1, MTX, or APAP for 10 days. Q-RT-PCR was performed after 7 and 10 days to assess mRNA expression levels of COL1A1 (A) and COL3A1 (B) in HSC MTs. Pro-Collagen 1A1 (C) and CTGF (D) release were measured in the supernatant after 3, 7 and 10 days. Red dashed lines represent baseline expression of untreated control. Floating bars represent median ± min max. Statistical analysis based on ordinary one-way ANOVA followed by Dunnett's multiple comparisons test, with $^{\#/+}$, $p \leq 0.05$; $^{\#\#/++}$, $p \leq 0.01$; $^{\#\#\#/+++}$, $p \leq 0.001$; $^{\#\#\#\#/++++}$, $p \leq 0.0001$. $^{\#}$ represents comparison to HepaRG//HSC controls and $^{+}$ represents comparison to HepaRG + THP-1//HSC controls of the respective timepoint. N = 3 – 4 (3 – 4 independent biological replicates with 1 – 2 technical replicates).

THP-1 containing cultures at day 7 (14.7- and 11.0-fold). After 10 days, CTGF remained elevated in TGF-β1 treated HepaRG//HSC cultures, while MTX reduced CTGF levels. Consistent with the activation observed in KE4 upon TGF-β1 treatment, TGF-β1-activated HSC induced remodeling of the ECM.

4. Discussion

Liver-related toxicity remains the main reason for post-market drug withdrawal and drug attrition during the development of new molecular entities, making it essential to develop more physiological-relevant liver models. In this work, we aimed at applying a microphysiological system to study liver fibrosis progression and mimicking the events described in the liver fibrosis AOP. A critical requirement for the development of quantitative AOP models is the ability to monitor cell-type specific responses and, ideally, to isolate individual cell types for downstream analysis. To address this, we employed the Akura™ Twin microplate platform, which offers several advantages over conventional co-culture models such as transwells: a favorable cell-to-volume ratio, compatibility with high-throughput and automated workflows, and a user-friendly design optimized for 3D cultures. The Akura™ Twin microplate features interconnected wells that allow pairs of MTs to communicate through shared medium, facilitating the investigation of dynamic, cell-type specific responses, while enabling easy recovery of individual MTs. In our setup, the plate was gently tilted at one-minute intervals – not to induce shear stress, but to promote intercellular communication by enhancing diffusion. This approach aligns with physiological conditions in the liver, where shear stress is naturally low (0.1 – 0.5 dyn/cm^2) (Li et al., 2021).

To model fibrogenesis, HepaRG MTs were cultured in indirect contact with HSC MTs via shared medium. In this experimental setup, hepatocellular damage and activation of stellate cells could be captured, but the model was devoid of inflammatory signals due to the lack of a cell type taking the role of the Kupffer cell. Thus, differentiated THP-1 were integrated into the HepaRG MTs to study the impact of the immune factors on specific key events. As HSCs are the key drivers of fibrosis progression it is crucial to understand the underlying mechanisms of their activation. Hence, we were interested to establish a model, in which HSCs could be easily recovered and processed for downstream analysis.

All setups were challenged for 10 days with the pro-fibrotic cytokine TGF-β1, the fibrotic test compound MTX and the hepatotoxicant APAP. Although TGF-β1 can directly activate HSCs, it also induces apoptosis in hepatocytes and polarizes KCs toward an alternatively activated M2-phenotype, amplifying fibrosis-related signalling (Gaitantzi et al., 2018; Horvat et al., 2017; Kossmann et al., 1992; Leask & Abraham,

2004; Sakai et al., 2019). Hence, we consider TGF-β1 a valid positive control to model the liver fibrosis AOP. To monitor parameters relevant to cell health during the experiments, we employed bioenzymatic sensors (Jobst) to measure glucose consumption and lactate production. The sensors, which can run on sample volumes as low as 1 μL, and allow automated, non-disruptive, high-frequency measurements, provided robust data. Glucose consumption remained constant for the HepaRG//HSC cultures over 10 days but integration of THP-1 increased the consumption of glucose over time in control and TGF-β1-treated conditions. The pattern of lactate production mirrored glucose consumption, reflecting the observed increased number of cells in THP-1-containing cultures for control and TGF-β1-treated conditions (Fig. S1, Fig. S2). Differentiated THP-1 typically lose their ability to proliferate (Liu et al., 2023). However, recent findings suggest that hypoxic conditions can trigger cell cycle re-entry in monocyte-derived macrophages (Meng et al., 2024). We therefore hypothesize that oxygen gradients within the HepaRG + THP-1 MTs may induce re-entry of THP-1 cells into the cell cycle (Hirschhaeuser et al., 2010). MTX- and APAP-treated cultures showed steady lactate production rates. This aligns with their known mode of action: MTX inhibits cell proliferation via cell cycle arrest, while APAP can induce apoptosis and mitochondrial dysfunction in monocytes and macrophages, thereby inhibiting proliferation (Brown et al., 2016; Raza & John, 2015).

Having shown that the MTs are viable and metabolically active over 10 days, we focused on the first key event of the liver fibrosis AOP: hepatocyte injury or death. To this end, we selected hepatocyte specific markers albumin and urea and measured their secretion. Across all setups, the control HepaRG ± THP-1 MTs secreted on average 17.6 ± 3.4 μg albumin/day/million cells. This value is lower than estimated levels in human (37–105 μg/day/million cells) but significantly outperforms standard 2D primary hepatocyte cultures (~1 μg/day/million cells) and is in agreement with existing MPS data (Baudy et al., 2020; Chang et al., 2017; Jellali et al., 2016; Prodanov et al., 2016). Consistent with their hepatotoxicity, TGF-β1 and APAP significantly suppressed albumin secretion from day 3 onward, while MTX reduced albumin only after day 7. Albumin production detected by immunostaining was also downregulated by TGF-β1 and APAP, but not by MTX, consistent with reports indicating that MTX has minimal effect on albumin levels in vivo (Shergy & Pisetsky, 1988; Tag, 2015). In some in vitro studies, MTX led to an upregulation of albumin after extended culture, likely due to compensatory mechanisms, e.g. secretion of factors supporting albumin synthesis (Norona et al., 2019). Interestingly, THP-1 integration slightly enhanced albumin production, suggesting a more physiologically relevant microenvironment (Norona et al., 2019). To cover the functionality of the hepatocellular mitochondria, urea synthesis was investigated (Baudy et al., 2020). Urea levels were maintained in HepaRG//HSC cultures, while like the effect observed for albumin, the integration of THP-1 cells resulted in a significantly higher urea release. In line with its reported mitochondrial toxicity, APAP markedly reduced urea levels in both setups (Umbaugh et al., 2021). MTX has also been shown to induce oxidative stress in mitochondria, however, only the cultures containing THP-1 cells were sensitive to MTX-induced injury (Mahmoud et al., 2017).

Next, we investigated KE2, the activation of the Kupffer cells. In a previous study using the same cell types, TREM2 and ALOX5AP were identified as activation markers of THP-1 that were upregulated upon fibrotic stimuli (Messner, Babrak, et al., 2021). ALOX5AP is a key regulator of proliferation and survival in Kupffer cells (Titos et al., 2003). Inhibition of ALOX5AP has been shown to reduce CCl_4-induced liver injury and to limit inflammatory infiltration in metabolic-associated fatty liver disease (MAFLD) (Brenner et al., 2013; Titos et al., 2005). TREM2 on the other hand, has been implied as a marker for "scar-associated macrophages" and is linked to hepatic portal fibrosis (Fabre et al., 2023; Govaere et al., 2023). TGF-β1 significantly increased the expression of both markers, confirming macrophage activation. In contrast, APAP suppressed both markers, while MTX had no significant effect. A recent study indicated that TREM2-positive macrophages promote tissue repair following APAP-induced damage (Coelho et al., 2021). The downregulation of TREM2 by APAP observed in our study suggests that APAP's acute toxicity precludes the immune repair response typically associated with TREM2-positive macrophages, underlining its non-fibrotic mechanism of toxicity.

Following successful activation of the THP-1 by TGF-β1 treatment, we moved on to investigate key event 3, the release of TGF-β1. Since exogeneous TGF-β1 was used in our study and would have been a confounding factor, we focused on the transcriptional regulation of TGF-β1 in THP-1 and on the release of the downstream marker PAI-1 in the cell culture supernatant. TGF-β1 treatment increased mRNA levels of TGF-β1 after 7 days, returning to baseline by day 10. This upregulation correlates with increased TGF-β1 expression levels observed in TREM2-positive mice macrophages (Jung et al., 2022). In addition, TGF-β1 is known to sustain macrophage function during tissue repair by autocrine signaling, creating a positive feedback loop (Patel et al., 2022). Both MTX and APAP suppressed TGF-β1 expression, indicating inhibition of the anti-inflammatory macrophage phenotype. This was unexpected for MTX, which typically targets pro-inflammatory macrophages (Municio et al., 2016). However, in a recent study using a bioprinted liver with incorporated Kupffer cells, the abundance of pro-inflammatory to anti-inflammatory cytokines changed over time (day 13 vs day 27), indicating that a longer time frame might be essential for MTX to induce anti-inflammatory polarization (Norona et al., 2019). PAI-1 is involved in the plasminogen pathway, which regulates protein synthesis and wound healing processes through fibrinolysis. It inhibits the conversion from plasminogen to plasmin and the activation of plasmin-dependent matrix metalloproteinases (MMPs) and thereby suppresses the breakdown of collagen and other ECM proteins (Ghosh & Vaughan, 2012). The expression of PAI-1 is tightly regulated by TGF-β1, making it an excellent downstream marker of TGF-β1 (Noguchi et al., 2020). As expected, PAI-1 levels increased in all TGF-β1-treated conditions, with significantly higher levels measured in THP-1-containing cultures, indicating an increased release of endogenous TGF-β1 by THP-1 and further supporting the role of THP-1 cells as a primary TGF-β1 source. We further validated this intercellular communication by measuring PAI-1 levels in HepaRG, THP-1 and hTERT-HSC monocultures and observed increased release of PAI-1 only in HepaRG and hTERT-HSC monocultures upon treatment with TGF-β1 (Fig. S4). This is in accordance with literature linking PAI-1 release mainly to hepatocytes, liver sinusoidal endothelial cells and HSCs, but not Kupffer cells (Knittel et al., 1996; Zhang et al., 1999).

Stellate cell activation, the fourth KE in this AOP, is characterized by the formation of stress fibers. Our data show that HSCs were markedly activated in TGF-β1-treated cultures, as determined by elevated ACTA2 and FN1 mRNA and higher protein levels of f-actin and fibronectin. Neither APAP nor MTX activated HSCs under these experimental conditions. This was surprising, as the combination of MTX and factors produced by HepaRG and THP-1 were expected to trigger the MTX-induced HSC-activation. The lack of HSC activation by MTX in this experimental setup may be related to insufficient amounts of activating factors reaching the HSC MTs, which warrants further investigations with different cell types or proportions. THP-1 cells have indeed been shown to secret fewer cytokines than activated primary Kupffer cells or primary blood monocytes (PBMCs) (Kermanizadeh et al., 2019). Thus, the released amounts of cytokines might have been insufficient to trigger HSC activation in the Akura™ Twin system. In our previously established model, in which MTX elicited a fibrotic response, HepaRG, THP-1 and hTERT-HSCs were cultured in direct contact. For future investigations based on indirect cell-to-cell contact, the use of primary KCs or PBMCs instead of THP-1 cells should be considered. Also, HSC are known to be easily activated in 2D but there is insufficient evidence regarding their behavior in more physiological conditions like 3D-MTs (Leite et al., 2016; Olsen et al., 2011). In fact, clinical evidence suggests that MTX alone is insufficient to trigger fibrosis without co-existing

metabolic conditions, such as diabetes mellitus Type II or obesity. The prevalence of MAFLD in patients with rheumatoid arthritis or psoriasis, for which MTX is commonly prescribed, is substantial (Atallah et al., 2023; Di Martino, 2023) and future in vitro models might require additional stressors, such as fatty acid pre-treatment, to more accurately assess the fibrogenic potential of new drugs in specific patient populations (Ramos et al., 2022; Saklayen, 2018).

Finally, we addressed the remodeling of the ECM described in key event 5 (KE5). TGF-β1 induced gene expression of COL1A1 and to a lesser extent that of COL3A1 in HSCs. In concordance with this, the protein levels of Pro-Collagen 1A1, a precursor of collagen Type I A1, were increased in the supernatant from day 7 onward after incubation with TGF-β1. As expected, and as a logical consequence of the results in the previous KE (KE4), MTX had no effect on Pro-Collagen 1A1, while APAP reduced its levels. We also measured CTGF, known to stimulate the deposition and the remodeling of ECM by myofibroblasts (Lipson et al., 2012). CTGF levels rose earlier than Pro-Collagen 1A1 following TGF-β1 exposure and remained elevated throughout, making it a useful biomarker to investigate early responses. This is in line with the biological function of CTGF that is primarily induced by transforming growth factor-β (TGF-β) in human skin fibroblasts and appears to function as a downstream mediator of TGF-β's ability to stimulate collagen synthesis. It has been reported that CTGF is both regulated by TGF-β signaling and is required for downstream action of TGF-β (Quan et al., 2010). In our experimental setups, THP-1 inclusion significantly enhanced CTGF expression, emphasizing the importance of cellular crosstalk between immune cells and HSCs (Fig. S3). Despite clear treatment-dependent trends, variability between biological replicates in absolute values of CTGF and Pro-Collagen 1A1 was high, similar to the heterogeneity observed in clinical CTGF levels in MAFLD patients with values ranging from 1028.3 – 11606.8 pmol/L (Kogiso et al., 2024).

From our data with human hepatic cells we can conclude that crosstalk between the cell types is important and that utilizing a microphysiological system like Akura™ Twin enables the performance of targeted experiments. Human cell lines are advantageous due to their availability, reproducibility and low cost. To further improve translational relevance, future studies should focus on the integration of primary cells or induced pluripotent stem cells into the system. A recent FDA study demonstrated a detection sensitivity of 72 % and a specificity of 78 % for "Most-DILI-concern" drugs using primary human liver microtissues, paving the way for reproducible follow up studies using primary cells also for the investigation of the fibrotic potential of a drug (Fäs et al., 2025). Additionally, the integration of liver sinusoidal endothelial cells (LSECs) could greatly enhance the performance of the system. During fibrogenesis, LSECs have been shown to secret different cytokines and chemokines, regulating not only HSC, but also KC activation (Horvat et al., 2017; Jang et al., 2019). In our hands, the more complex model including THP-1-derived macrophages emerged as the most physiologically relevant, particularly in preserving hepatocellular function, demonstrating high sensitivity to hepatocellular injury, and fully recapitulating the liver fibrosis AOP cascade triggered by TGF-β1. The Akura™ Twin microplate, a high-throughput microphysiological system, allowed us to successfully model and measure the key events of liver fibrosis by integrating HepaRG, THP-1, and hTERT-HSC cells. Specific markers were identified for each key event: albumin and urea for hepatocyte function (KE1), TREM2 and ALOX5AP for macrophage (Kupffer cell) activation (KE2), TGF-β1 mRNA and PAI-1 protein for pro-fibrotic signaling (KE3), αSMA, f-actin, and fibronectin for HSC activation (KE4), and Pro-Collagen 1A1 and CTGF for ECM remodeling (KE5). The experimental setup enabled a longitudinal study, cell-cell communication and quantification of cellular responses, all key elements for the implementation of quantitative AOPs. Hence, this platform provides a valuable toolbox for toxicity assessment and contributes toward the development of regulatory-accepted in vitro models in preclinical drug development. Regarding MTX-induced fibrosis, the inclusion of THP-1 cells was insufficient to trigger MTX-induced fibrosis in this system. This may reflect a lack of adequate or synergistic stimuli required to mimic the clinical situation. Alternatively, the lack of direct cell-cell contact in our current setup may limit fibrogenic signaling, as previous studies using 3D multicellular MTs have shown MTX-induced fibrosis (Messner et al., 2021a,b; Prestigiacomo et al., 2017). Further studies using similar approaches should be conducted to identify additional factors contributing to MTX-induced fibrosis in humans, which only occurs in a small number of patients in the clinic (3.3 % in rheumatoid arthritis patients) and might have been historically overestimated (AkbariRad et al., 2025; Atallah et al., 2023; Di Martino, 2023; Turner et al., 2020).

Funding sources

This research was funded by the Swiss National Science Foundation (SNF) grant No. 40B2–0187219, by the Swiss Centre for Applied Human Toxicology (SCAHT), and the Institute for Chemistry and Bioanalytics at the University of Applied Sciences and Arts Northwestern Switzerland (FHNW).

CRediT authorship contribution statement

Saskia Schmidt: Writing – review & editing, Writing – original draft, Visualization, Project administration, Methodology, Investigation, Formal analysis, Data curation, Conceptualization. **Laura Suter-Dick:** Writing – review & editing, Writing – original draft, Supervision, Resources, Project administration, Funding acquisition, Conceptualization.

Declaration of Competing Interest

The authors declare that they have no known competing financial interests or personal relationships that could have appeared to influence the work reported in this paper.

The author is an Editorial Board Member/Editor-in-Chief/Associate Editor/Guest Editor for this journal and was not involved in the editorial review or the decision to publish this article.

Acknowledgments

We would like to thank B. Schnabl for providing us with the hTERT-HSC and Biopredic International for supplying the HepaRG cells. In addition, we would like to thank InSpheroAG for providing the Akura™ Twin system and Lisa Hoelting for consulting and reviewing the manuscript.

Appendix A. Supporting information

Supplementary data associated with this article can be found in the online version at doi:10.1016/j.tox.2025.154248.

Data availability

Data will be made available on request.

References

AkbariRad, M., Rezaieyazdi, Z., Tajik, A., Ataei, B., Sarabi, M., MehradMajd, H., Vossoughinia, H., Firoozi, A., 2025. The relationship between dose of methotrexate and incidence of liver fibrosis in patients with rheumatoid arthritis. Rheumatology. https://doi.org/10.5114/reum/199740.

Angulo, P., Kleiner, D.E., Dam-Larsen, S., Adams, L.A., Bjornsson, E.S., Charatcharoenwitthaya, P., Mills, P.R., Keach, J.C., Lafferty, H.D., Stahler, A., Haflidadottir, S., Bendtsen, F., 2015. Liver fibrosis, but no other histologic features, is associated with Long-term outcomes of patients with nonalcoholic fatty liver disease. Gastroenterology 149 (2), 389–397.e10. https://doi.org/10.1053/j.gastro.2015.04.043.

Atallah, E., Grove, J.I., Crooks, C., Burden-Teh, E., Abhishek, A., Moreea, S., Jordan, K. M., Ala, A., Hutchinson, D., Aspinall, R.J., Murphy, R., Aithal, G.P., 2023. Risk of

liver fibrosis associated with long-term methotrexate therapy May be overestimated. J. Hepatol. 78 (5), 989–997. https://doi.org/10.1016/j.jhep.2022.12.034.
Babai, S., Auclert, L., Le-Louët, H., 2021. Safety data and withdrawal of hepatotoxic drugs. Therapies 76 (6), 715–723. https://doi.org/10.1016/j.therap.2018.02.004.
Baudy, A.R., Otieno, M.A., Hewitt, P., Gan, J., Roth, A., Keller, D., Sura, R., Van Vleet, T. R., Proctor, W.R., 2020. Liver microphysiological systems development guidelines for safety risk assessment in the pharmaceutical industry. Lab a Chip 20 (2), 215–225. https://doi.org/10.1039/c9lc00768g.
Bircsak, K.M., DeBiasio, R., Miedel, M., Alsebahi, A., Reddinger, R., Saleh, A., Shun, T., Vernetti, L.A., Gough, A., 2021. A 3D microfluidic liver model for high throughput compound toxicity screening in the OrganoPlate®. Toxicology 450, 152667. https://doi.org/10.1016/j.tox.2020.152667.
Bonanini, F., Dinkelberg, R., Torregrosa, M.C., Kortekaas, N., Hagens, T.M.S., Treillard, S., Kurek, D., Van Duinen, V., Vulto, P., Bircsak, K., 2025. A microvascularized in vitro liver model for disease modeling and drug discovery. Biofabrication 17 (1), 015007. https://doi.org/10.1088/1758-5090/ad818a.
Brenner, C., Galluzzi, L., Kepp, O., Kroemer, G., 2013. Decoding cell death signals in liver inflammation. J. Hepatol. 59 (3), 583–594. https://doi.org/10.1016/j.jhep.2013.03.033.
Brown, P.M., Pratt, A.G., Isaacs, J.D., 2016. Mechanism of action of methotrexate in rheumatoid arthritis, and the search for biomarkers. Nat. Rev. Rheumatol. 12 (12), 731–742. https://doi.org/10.1038/nrrheum.2016.175.
Casati, S., Asturiol, D., Browne, P., Kleinstreuer, N., Régimbald-Krnel, M., Therriault, P., 2022. Standardisation and international adoption of defined approaches for skin sensitisation. Front. Toxicol. 4, 943152. https://doi.org/10.3389/ftox.2022.943152.
Chang, S.-Y., Voellinger, J.L., Van Ness, K.P., Chapron, B., Shaffer, R.M., Neumann, T., White, C.C., Kavanagh, T.J., Kelly, E.J., Eaton, D.L., 2017. Characterization of rat or human hepatocytes cultured in microphysiological systems (MPS) to identify hepatotoxicity. Toxicol. Vitr. 40, 170–183. https://doi.org/10.1016/j.tiv.2017.01.007.
Cheng, H., Rademaker, M., 2018. Monitoring methotrexate-induced liver fibrosis in patients with psoriasis: utility of transient elastography. Psoriasis. Targets Ther. 8, 21–29. https://doi.org/10.2147/PTT.S141629.
Cho, H.J., Kim, H.J., Lee, K.J., Lasli, S., Ung, A., Hoffman, T., Nasiri, R., Bandaru, P., Ahadian, S., Dokmeci, M.R., Lee, J., Khademhosseini, A., 2021. Bioengineered multicellular liver microtissues for modeling advanced hepatic fibrosis driven through Non-Alcoholic fatty liver disease. Small 17 (14). https://doi.org/10.1002/smll.202007425.
Coelho, I., Duarte, N., Barros, A., Macedo, M.P., Penha-Gonçalves, C., 2021. Trem-2 promotes emergence of restorative macrophages and endothelial cells during recovery from hepatic tissue damage. Front. Immunol. 11, 616044. https://doi.org/10.3389/fimmu.2020.616044.
Dalsbecker, P., Beck Adiels, C., Goksör, M., 2022. Liver-on-a-chip devices: the pros and cons of complexity. Am. J. Physiol. Gastrointest. Liver Physiol. 323 (3), G188–G204. https://doi.org/10.1152/ajpgi.00346.2021.
Di Martino, V., 2023. Methotrexate-induced liver fibrosis: the end of a long-held belief. J. Hepatol. 78 (5), 896–897. https://doi.org/10.1016/j.jhep.2023.02.018.
Edwards, M., Blanquie, O., Ehmann, F., 2025. Insights into new approach methodology innovation: an EMA perspective. Nat. Rev. Drug Discov. https://doi.org/10.1038/d41573-025-00052-8.
Fabre, T., Barron, A.M.S., Christensen, S.M., Asano, S., Bound, K., Lech, M.P., Wadsworth, M.H., Chen, X., Wang, C., Wang, J., McMahon, J., Schlerman, F., White, A., Kravarik, K.M., Fisher, A.J., Borthwick, L.A., Hart, K.M., Henderson, N.C., Wynn, T.A., Dower, K., 2023. Identification of a broadly fibrogenic macrophage subset induced by type 3 inflammation. Sci. Immunol. 8 (82), eadd8945. https://doi.org/10.1126/sciimmunol.add8945.
Fäs, L., Chen, M., Tong, W., Wenz, F., Hewitt, N.J., Tu, M., Sanchez, K., Zapiórkowska-Blumer, N., Varga, H., Kaczmarska, K., Colombo, M.V., Filippi, B.G.H., 2025. Physiological liver microtissue 384-well microplate system for preclinical hepatotoxicity assessment of therapeutic small molecule drugs. Toxicol. Sci. 203 (1), 79–87. https://doi.org/10.1093/toxsci/kfae123.
Gaitantzi, H., Meyer, C., Rakoczy, P., Thomas, M., Wahl, K., Wandrer, F., Bantel, H., Alborzinia, H., Wölfl, S., Ehnert, S., Nüssler, A., Bergheim, I., Ciuclan, L., Ebert, M., Breitkopf-Heinlein, K., Dooley, S., 2018. Ethanol sensitizes hepatocytes for TGF-β-triggered apoptosis. Cell Death Dis. 9 (2). https://doi.org/10.1038/s41419-017-0071-y.
Ghosh, A.K., Vaughan, D.E., 2012. PAI-1 in tissue fibrosis. J. Cell. Physiol. 227 (2), 493–507. https://doi.org/10.1002/jcp.22783.
Govaere, O., Hasoon, M., Alexander, L., Cockell, S., Tiniakos, D., Ekstedt, M., Schattenberg, J.M., Boursier, J., Bugianesi, E., Ratziu, V., Investigators, L.I.T.M.U.S., Daly, A.K., Anstee, Q.M., 2023. A proteo-transcriptomic map of non-alcoholic fatty liver disease signatures. Nat. Metab. 5 (4), 572–578. https://doi.org/10.1038/s42255-023-00775-1.
Hirschhaeuser, F., Menne, H., Dittfeld, C., West, J., Mueller-Klieser, W., Kunz-Schughart, L.A., 2010. Multicellular tumor spheroids: an underestimated tool is catching up again. J. Biotechnol. 148 (1), 3–15. https://doi.org/10.1016/j.jbiotec.2010.01.012.
Horvat, T., Landesmann, B., Lostia, A., Vinken, M., Munn, S., Whelan, M., 2017. Adverse outcome pathway development from protein alkylation to liver fibrosis. Arch. Toxicol. 91 (4), 1523–1543. https://doi.org/10.1007/s00204-016-1814-8.
Ingber, D.E., 2022. Human organs-on-chips for disease modelling, drug development and personalized Medicine. Nat. Rev. Genet. 23 (8), 467–491. https://doi.org/10.1038/s41576-022-00466-9.
Jaeschke, H., Akakpo, J.Y., Umbaugh, D.S., Ramachandran, A., 2020. Novel therapeutic approaches against Acetaminophen-induced liver injury and acute liver failure. Toxicol. Sci. 174 (2), 159–167. https://doi.org/10.1093/toxsci/kfaa002.
Jang, K.-J., Otieno, M.A., Ronxhi, J., Lim, H.-K., Ewart, L., Kodella, K.R., Petropolis, D.B., Kulkarni, G., Rubins, J.E., Conegliano, D., Nawroth, J., Simic, D., Lam, W., Singer, M., Barale, E., Singh, B., Sonee, M., Streeter, A.J., Manthey, C., Hamilton, G. A., 2019. Reproducing human and cross-species drug toxicities using a Liver-Chip. Sci. Transl. Med. 11 (517), eaax5516. https://doi.org/10.1126/scitranslmed.aax5516.
Jellali, R., Bricks, T., Jacques, S., Fleury, M., Paullier, P., Merlier, F., Leclerc, E., 2016. Long-term human primary hepatocyte cultures in a microfluidic liver biochip show maintenance of mRNA levels and higher drug metabolism compared with petri cultures. Biopharm. Drug Dispos. 37 (5), 264–275. https://doi.org/10.1002/bdd.2010.
Josse, R., Dumont, J., Fautrel, A., Robin, M.-A., Guillouzo, A., 2012. Identification of early target genes of aflatoxin B1 in human hepatocytes, inter-individual variability and comparison with other genotoxic compounds. Toxicol. Appl. Pharmacol. 258 (2), 176–187. https://doi.org/10.1016/j.taap.2011.10.019.
Jung, S.-H., Hwang, B.-H., Shin, S., Park, E.-H., Park, S.-H., Kim, C.W., Kim, E., Choo, E., Choi, I.J., Swirski, F.K., Chang, K., Chung, Y.-J., 2022. Spatiotemporal dynamics of macrophage heterogeneity and a potential function of Trem2hi macrophages in infarcted hearts. Nat. Commun. 13 (1), 4580. https://doi.org/10.1038/s41467-022-32284-2.
Kanabekova, P., Kadyrova, A., Kulsharova, G., 2022. Microfluidic Organ-on-a-Chip devices for liver disease modeling in vitro. Micromachines 13 (3), 428. https://doi.org/10.3390/mi13030428.
Kermanizadeh, A., Brown, D.M., Stone, V., 2019. The variances in cytokine production profiles from non- or activated THP-1, kupffer cell and human blood derived primary macrophages following exposure to either alcohol or a panel of engineered nanomaterials. PLOS ONE 14 (8), e0220974. https://doi.org/10.1371/journal.pone.0220974.
Knittel, T., Fellmer, P., Ramadori, G., 1996. Gene expression and regulation of plasminogen activator inhibitor type I in hepatic stellate cells of rat liver. Gastroenterology 111 (3), 745–754. https://doi.org/10.1053/gast.1996.v111.pm8780581.
Kogiso, T., Takayanagi, K., Ishizuka, T., Otsuka, M., Inai, K., Ogasawara, Y., Horiuchi, K., Taniai, M., Tokushige, K., 2024. Serum level of full-length connective tissue growth factor reflects liver fibrosis stage in patients with Fontan-associated liver disease. PLOS ONE 19 (1), e0296375. https://doi.org/10.1371/journal.pone.0296375.
Kossmann, T., Manthey, C.L., Brandes, M.E., Morganti-Kossmann, M.C., Ohura, K., Allen, J.B., Mergenhagen, S.E., Wahl, S.M., 1992. Kupffer cells express type I TGF-βReceptors, migrate to TGF-βand participate in streptococcal cell wall induced hepatic granuloma formation. Growth Factors 7 (1), 73–83. https://doi.org/10.3109/08977199209023939.
Kostrzewski, T., Snow, S., Battle, A.L., Peel, S., Ahmad, Z., Basak, J., Surakala, M., Bornot, A., Lindgren, J., Ryaboshapkina, M., Clausen, M., Lindén, D., Maass, C., Young, L.M., Corrigan, A., Ewart, L., Hughes, D., 2021. Modelling human liver fibrosis in the context of non-alcoholic steatohepatitis using a microphysiological system. Commun. Biol. 4 (1), 1080. https://doi.org/10.1038/s42003-021-02616-x.
Kullak-Ublick, G.A., Andrade, R.J., Merz, M., End, P., Benesic, A., Gerbes, A.L., Aithal, G. P., 2017. Drug-induced liver injury: recent advances in diagnosis and risk assessment. Gut 66 (6), 1154–1164. https://doi.org/10.1136/gutjnl-2016-313369.
Leask, A., Abraham, D.J., 2004. TGF-β signaling and the fibrotic response. FASEB J. 18 (7), 816–827. https://doi.org/10.1096/fj.03-1273rev.
Leite, S.B., Roosens, T., El Taghdouini, A., Mannaerts, I., Smout, A.J., Najimi, M., Sokal, E., Noor, F., Chesne, C., van Grunsven, L.A., 2016. Novel human hepatic organoid model enables testing of drug-induced liver fibrosis in vitro. Biomaterials 78, 1–10. https://doi.org/10.1016/j.biomaterials.2015.11.026.
Lertnawapan, R., Chonprasertsuk, S., Siramolpiwat, S., Jatuworapruk, K., 2023. Correlation between cumulative methotrexate dose, metabolic syndrome and hepatic fibrosis detected by FibroScan in rheumatoid arthritis patients. Medicina 59 (6), 1029. https://doi.org/10.3390/medicina59061029.
Li, W., Li, P., Li, N., Du, Y., Lü, S., Elad, D., Long, M., 2021. Matrix stiffness and shear stresses modulate hepatocyte functions in a fibrotic liver sinusoidal model. Am. J. Physiol. Gastrointest. Liver Physiol. 320 (3), G272–G282. https://doi.org/10.1152/ajpgi.00379.2019.
Lipson, K.E., Wong, C., Teng, Y., Spong, S., 2012. CTGF is a central mediator of tissue remodeling and fibrosis and its inhibition can reverse the process of fibrosis. Fibrogenes. Tissue Repair 5 (S1), S24. https://doi.org/10.1186/1755-1536-5-S1-S24.
Liu, T., Huang, T., Li, J., Li, A., Li, C., Huang, X., Li, D., Wang, S., Liang, M., 2023. Optimization of differentiation and transcriptomic profile of THP-1 cells into macrophage by PMA. PLOS ONE 18 (7), e0286056. https://doi.org/10.1371/journal.pone.0286056.
MacDonald, A., Burden, A.D., 2005. Noninvasive monitoring for methotrexate hepatotoxicity. Br. J. Dermatol. 152 (3), 405–408. https://doi.org/10.1111/j.1365-2133.2005.06605.x.
Mahmoud, A.M., Hussein, O.E., Hozayen, W.G., Abd El-Twab, S.M., 2017. Methotrexate hepatotoxicity is associated with oxidative stress, and down-regulation of PPARγ and Nrf2: protective effect of 18β-Glycyrrhetinic acid. Chem. Biol. Interact. 270, 59–72. https://doi.org/10.1016/j.cbi.2017.04.009.
Meng, B., Zhao, N., Mlcochova, P., Ferreira, I.A.T.M., Ortmann, B.M., Davis, T., Wit, N., Rehwinkel, J., Cook, S., Maxwell, P.H., Nathan, J.A., Gupta, R.K., 2024. Hypoxia drives HIF2-dependent reversible macrophage cell cycle entry. Cell Rep. 43 (7), 114471. https://doi.org/10.1016/j.celrep.2024.114471.
Messner, C.J., Babrak, L., Titolo, G., Caj, M., Miho, E., Suter-Dick, L., 2021a. Single cell gene expression analysis in a 3D microtissue liver model reveals cell Type-Specific responses to Pro-Fibrotic TGF-β1 stimulation. Int. J. Mol. Sci. 22 (9), 4372. https://doi.org/10.3390/ijms22094372. PMID: 33922101; PMCID: PMC8122664.

Messner, C.J., Schmidt, S., Özkul, D., Gaiser, C., Terracciano, L., Krähenbühl, S., Suter-Dick, L., 2021b. Identification of miR-199a-5p, miR-214-3p and miR-99b-5p as Fibrosis-Specific extracellular biomarkers and promoters of HSC activation. Int. J. Mol. Sci. 22 (18), 9799. https://doi.org/10.3390/ijms22189799.

Mikkelsen, T.S., Thorn, C.F., Yang, J.J., Ulrich, C.M., French, D., Zaza, G., Dunnenberger, H.M., Marsh, S., McLeod, H.L., Giacomini, K., Becker, M.L., Gaedigk, R., Leeder, J.S., Kager, L., Relling, M.V., Evans, W., Klein, T.E., Altman, R. B., 2011. PharmGKB summary: methotrexate pathway. Pharm. Genom. 21 (10), 679–686. https://doi.org/10.1097/FPC.0b013e328343dd93.

Municio, C., Soler Palacios, B., Estrada-Capetillo, L., Benguria, A., Dopazo, A., García-Lorenzo, E., Fernández-Arroyo, S., Joven, J., Miranda-Carús, M.E., González-Álvaro, I., Puig-Kröger, A., 2016. Methotrexate selectively targets human proinflammatory macrophages through a thymidylate synthase/p53 axis. Ann. Rheum. Dis. 75 (12), 2157–2165. https://doi.org/10.1136/annrheumdis-2015-208736.

Noguchi, R., Kaji, K., Namisaki, T., Moriya, K., Kawaratani, H., Kitade, M., Takaya, H., Aihara, Y., Douhara, A., Asada, K., Nishimura, N., Miyata, T., Yoshiji, H., 2020. Novel oral plasminogen activator inhibitor-1 inhibitor TM5275 attenuates hepatic fibrosis under metabolic syndrome via suppression of activated hepatic stellate cells in rats. Mol. Med. Rep. https://doi.org/10.3892/mmr.2020.11360.

Norona, L.M., Nguyen, D.G., Gerber, D.A., Presnell, S.C., Mosedale, M., Watkins, P.B., 2019. Bioprinted liver provides early insight into the role of kupffer cells in TGF-β1 and methotrexate-induced fibrogenesis. PLOS ONE 14 (1), e0208958. https://doi.org/10.1371/journal.pone.0208958.

Olsen, A.L., Bloomer, S.A., Chan, E.P., Gaça, M.D.A., Georges, P.C., Sackey, B., Uemura, M., Janmey, P.A., Wells, R.G., 2011. Hepatic stellate cells require a stiff environment for myofibroblastic differentiation. Am. J. Physiol. Gastrointest. Liver Physiol. 301 (1), G110–G118. https://doi.org/10.1152/ajpgi.00412.2010.

Patel, N.K., Nunez, J.H., Sorkin, M., Marini, S., Pagani, C.A., Strong, A.L., Hwang, C.D., Li, S., Padmanabhan, K.R., Kumar, R., Bancroft, A.C., Greenstein, J.A., Nelson, R., Rasheed, H.A., Livingston, N., Vasquez, K., Huber, A.K., Levi, B., 2022. Macrophage TGF-β signaling is critical for wound healing with heterotopic ossification after trauma. JCI Insight 7 (20), e144925. https://doi.org/10.1172/jci.insight.144925.

Pellicoro, A., Ramachandran, P., Iredale, J.P., Fallowfield, J.A., 2014. Liver fibrosis and repair: immune regulation of wound healing in a solid organ. Nat. Rev. Immunol. 14 (3), 181–194. https://doi.org/10.1038/nri3623.

Prestigiacomo, V., Weston, A., Messner, S., Lampart, F., Suter-Dick, L., 2017. Pro-fibrotic compounds induce stellate cell activation, ECM-remodelling and Nrf2 activation in a human 3D-multicellular model of liver fibrosis. PLOS ONE 12 (6), e0179995. https://doi.org/10.1371/journal.pone.0179995.

Prodanov, L., Jindal, R., Bale, S.S., Hegde, M., McCarty, W.J., Golberg, I., Bhushan, A., Yarmush, M.L., Usta, O.B., 2016. Long-term maintenance of a microfluidic 3D human liver sinusoid. Biotechnol. Bioeng. 113 (1), 241–246. https://doi.org/10.1002/bit.25700.

Quan, T., Shao, Y., He, T., Voorhees, J.J., Fisher, G.J., 2010. Reduced expression of connective tissue growth factor (CTGF/CCN2) mediates collagen loss in chronologically aged human skin. J. Invest. Dermatol. 130 (2), 415–424. https://doi.org/10.1038/jid.2009.224.

Ramos, M.J., Bandiera, L., Menolascina, F., Fallowfield, J.A., 2022. In vitro models for non-alcoholic fatty liver disease: emerging platforms and their applications. iScience 25 (1), 103549. https://doi.org/10.1016/j.isci.2021.103549.

Raza, H., John, A., 2015. Differential cytotoxicity of acetaminophen in mouse macrophage J774.2 and human hepatoma HepG2 cells: protection by diallyl sulfide. PLOS ONE 10 (12), e0145965. https://doi.org/10.1371/journal.pone.0145965.

Roberts, R.A., 2024. New approach methodologies (NAMs) in drug safety assessment: a vision of the future. Curr. Opin. Toxicol. 40, 100502. https://doi.org/10.1016/j.cotox.2024.100502.

Rubin, K., Janefeldt, A., Andersson, L., Berke, Z., Grime, K., Andersson, T.B., 2015. HepaRG cells as Human-Relevant in vitro model to study the effects of inflammatory stimuli on cytochrome P450 isoenzymes. Drug Metab. Dispos. 43 (1), 119–125. https://doi.org/10.1124/dmd.114.059246.

Sakai, M., Troutman, T.D., Seidman, J.S., Ouyang, Z., Spann, N.J., Abe, Y., Ego, K.M., Bruni, C.M., Deng, Z., Schlachetzki, J.C.M., Nott, A., Bennett, H., Chang, J., Vu, B.T., Pasillas, M.P., Link, V.M., Texari, L., Heinz, S., Thompson, B.M., Glass, C.K., 2019. Liver-Derived signals sequentially reprogram myeloid enhancers to initiate and maintain kupffer cell identity. Immunity 51 (4), 655–670.e8. https://doi.org/10.1016/j.immuni.2019.09.002.

Saklayen, M.G., 2018. The global epidemic of the metabolic syndrome. Curr. Hypertens. Rep. 20 (2), 12. https://doi.org/10.1007/s11906-018-0812-z.

Scheinpflug, J., Höfer, C.T., Schmerbeck, S.S., Steinfath, M., Doka, J., Tesfahunegn, Y.A., Violet, N., Renko, K., Gulich, K., John, T., Schneider, M.R., Wistorf, E., Schönfelder, G., Schulze, F., 2023. A microphysiological system for studying human bone biology under simultaneous control of oxygen tension and mechanical loading. Lab a Chip 23 (15), 3405–3423. https://doi.org/10.1039/D3LC00154G.

Schnabl, B., Choi, Y.H., Olsen, J.C., Hagedorn, C.H., & Brenner, D.A. (2002). Immortal Activated Human Hepatic Stellate Cells Generated by Ectopic Telomerase Expression.

Shergy, W., & Pisetsky, D. (1988). Methotrexate-Associated Hepatotoxicity: Retrospective Analysis of 210 Patients with Rheumatoid Arthritis. 85, 4.

Tag, H.M., 2015. Hepatoprotective effect of mulberry (Morus nigra) leaves extract against methotrexate induced hepatotoxicity in Male albino rat. BMC Complement. Altern. Med. 15 (1), 252. https://doi.org/10.1186/s12906-015-0744-y.

Titos, E., Clària, J., Planagumà, A., López-Parra, M., González-Périz, A., Gaya, J., Miquel, R., Arroyo, V., Rodés, J., 2005. Inhibition of 5-lipoxygenase-activating protein abrogates experimental liver injury: role of kupffer cells. J. Leukoc. Biol. 78 (4), 871–878. https://doi.org/10.1189/jlb.1204747.

Titos, E., Clària, J., Planagumà, A., López-Parra, M., Villamor, N., Párrizas, M., Carrió, A., Miquel, R., Jiménez, W., Arroyo, V., Rivera, F., Rodés, J., 2003. Inhibition of 5-lipoxygenase induces cell growth arrest and apoptosis in rat kupffer cells: implications for liver fibrosis. FASEB J. 17 (12), 1745–1747. https://doi.org/10.1096/fj.02-1157fje.

Turner, L., Bland, M., Millson, C., Veysey, M., Hutchinson, J., 2020. O11 methotrexate: an innocent bystander in the development of liver fibrosis, findings of the STrATIFY study. Abstracts A6–A7. https://doi.org/10.1136/gutjnl-2020-BASL.11.

Umbaugh, D.S., Nguyen, N.T., Jaeschke, H., Ramachandran, A., 2021. Mitochondrial membrane potential drives early change in mitochondrial morphology after acetaminophen exposure. Toxicol. Sci. 180 (1), 186–195. https://doi.org/10.1093/toxsci/kfaa188.

Vinken, M., 2024. Adverse outcome pathway networks as the basis for the development of new approach methodologies: liver toxicity as a case study. Curr. Opin. Toxicol. 40, 100504. https://doi.org/10.1016/j.cotox.2024.100504.

Wu, Y., Geng, X., Wang, J., Miao, Y., Lu, Y., Li, B., 2016. The HepaRG cell line, a superior in vitro model to L-02, HepG2 and hiheps cell lines for assessing drug-induced liver injury. Cell Biol. Toxicol. 23.

Yoon, E., Babar, A., Choudhary, M., Kutner, M., Pyrsopoulos, N., 2016. Acetaminophen-induced hepatotoxicity: a comprehensive update. J. Clin. Transl. Hepatol. 4 (2), 131–142. https://doi.org/10.14218/JCTH.2015.00052.

Zhang, L.P., Takahara, T., Yata, Y., Furui, K., Jin, B., Kawada, N., Watanabe, A., 1999. Increased expression of plasminogen activator and plasminogen activator inhibitor during liver fibrogenesis of rats: role of stellate cells. J. Hepatol. 31 (4), 703–711. https://doi.org/10.1016/S0168-8278(99)80351-1.